Optics & Laser Technology 193 (2026) 114232

Contents lists available at ScienceDirect

Optics and Laser Technology

journal homepage: www.elsevier.com/locate/optlastec

Full length article

Polarization-dependent formation of side channels during percussion drilling with ultrafast lasers observed by means of high-speed X-ray imaging

Lukas Schneller [a,b,*], Manuel Henn [a], Marc Hummel [c,d], Christoph Spurk [c], Felix Beckmann [e], Julian Moosmann [e], Alexander Olowinsky [d], Daniel Holder [a], Christian Hagenlocher [a], Thomas Graf [a]

[a] Institut für Strahlwerkzeuge IFSW, University Stuttgart, Pfaffenwaldring 43, 70569 Stuttgart Germany
[b] Graduate School of Excellence advanced Manufacturing Engineering (GSaME) Nobelstr. 12, 70569 Stuttgart Germany
[c] RWTH Aachen University, Chair for Laser Technology LLT, Steinbachstr. 15, 52074 Aachen, Germany
[d] Fraunhofer-Institute for Laser Technology ILT, Steinbachstr. 15, 52074 Aachen, Germany
[e] Institute of Materials Physics, Helmholtz-Zentrum Hereon, Max-Planck-Str. 1, 21502 Geesthacht, Germany

ARTICLE INFO

Keywords:
Laser percussion drilling
High-speed X-ray imaging
Polarization
Side channel formation
Laser-material interaction
Borehole geometry, laser drilled hole quality

ABSTRACT

The side channels that occur during percussion drilling in stainless steel with ultrafast lasers with linear or circular polarization were observed using high-speed X-ray imaging, capturing the dynamic process in real-time and thus providing primary insights into their formation dynamics. We identified two distinct phenomena directly linked to the formation of side channels: (1) deflection of the borehole tip and (2) melt-induced obstructions that alter the propagation of the laser radiation. These phenomena can occur independently of each other and strongly depend on the state of polarization. With linear polarization, the side channels consistently form in the plane perpendicular to the direction of polarization, while the side channels occur without any preferred orientation when drilling with circular polarization. Additionally, the first side channels form at greater depths when higher pulse energies are applied. This study improves our understanding of the complex interplay between the state of polarization, melt dynamics, and side channel formation. The findings provide valuable information for optimizing laser drilling processes, particularly for high-aspect-ratio hole drilling with high pulse energies, and have promising applications in precision micromachining and industrial laser processing.

1. Introduction

Laser percussion drilling is commonly used to generate holes with high aspect ratios, such as those required for cooling channels in gas turbines [1] and aeroengines [2] or lubricant holes in tools for dry metal forming [3]. The creation of side channels and other geometry deviations during the drilling process often coincides with the formation of multiple hole exits and non-circular hole shapes, as shown in Fig. 1.

To date, in situ process imaging of the evolution of the borehole's shape has only been reported for transparent materials such as silicon [4], borosilicate glass [5,6], CVD diamond [7] and PMMA [8]. In the case of stainless steel, the borehole geometry could only be accessed by means of metallographically prepared cross sections of the samples [9] or the analysis of the resulting inlet and outlet of the completed holes [10]. However, in-process observation of the temporal evolution of the drilled hole, which also reveals the transient effects leading to the formation of side channels is not possible with these methods.

Techniques such as "drilling behind glass" [11–13] allow the in-situ observation of the borehole's geometry during the drilling process by replacing half of the sample with glass. Unfortunately, this approach strongly affects the process itself as a result of the significant differences in the optical and thermophysical properties of the materials involved.

Previous studies have shown that melt films are created on the walls of the holes even when drilling with ultrashort laser pulses. When melt is transported upwards from a deeper area of the borehole, as shown by Michalowski et al. [14], it can redeposit inhomogeneously on the borehole's wall and solidify as a recast layer that results in local geometric deviations inside the borehole [13–22]. Subsequent pulses may

* Corresponding author at: Institut für Strahlwerkzeuge IFSW, University Stuttgart, Pfaffenwaldring 43, 70569 Stuttgart Germany.
E-mail address: lukas.schneller@ifsw.uni-stuttgart.de (L. Schneller).

https://doi.org/10.1016/j.optlastec.2025.114232
Received 3 June 2025; Received in revised form 15 October 2025; Accepted 30 October 2025
Available online 7 November 2025

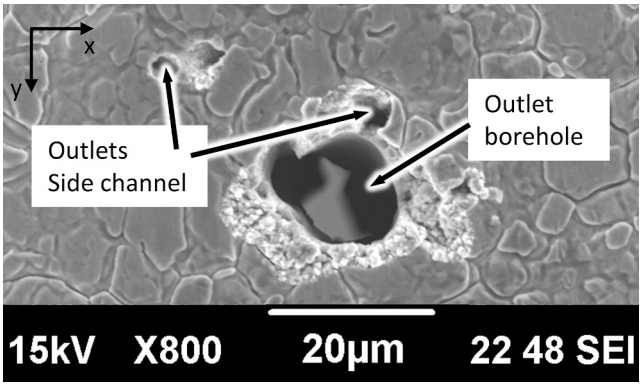

Fig. 1. Multiple outlets of a percussion-drilled through hole in stainless steel.

remove these material accumulations, resulting in a dynamic change of the borehole's geometry as shown by Zhao et al. [17].

When drilling with a linearly polarized laser beam, lateral deviations in the borehole geometry occur in the direction perpendicular to the orientation of the polarization, particularly in holes with high aspect ratios [8,18,23–29]. Side channels created in this way have been directly observed in diamond [30]. At the outlet of micro-holes, bulges in the hole profile have been observed that form perpendicular to the orientation of the polarization for various materials such as stainless-steel [25], copper, and titanium [24]. The authors attributed the appearance of these bulges to an inhomogeneous intensity distribution inside the hole due to the polarization-dependent absorption of the laser beam. At the inlet of the boreholes, the geometry was observed to be elongated in the direction of polarization [24,28,31,32].

So far it has not been clear how these side channels are created and how their position and direction can be influenced during the laser process.

Synchrotron X-ray imaging has been used to observe the laser drilling process in metals. Henn et al. were able to detect side channels during drilling with circular polarization [33]. Buser et al. used synchrotron X-ray imaging to validate OCT depth measurements [34].

With the experimental techniques employed in the present study it was possible, for the first time, to record the formation of side channels in high aspect ratio boreholes and to determine the position and direction of their growth depending on polarization and pulse energy.

2. Materials and methods

The experiments were conducted at the "PETRA III" facility of the German Electron Synchrotron (DESY) in Hamburg, Germany [35]. The experimental setup is identical to the setup used in [33] and [34] and shown in Fig. 2. The specifications of the imaging setup are described in detail by Wagner et al. [36] for investigating the laser welding process.

The ultra-short laser pulses were focused on the surface of the stainless steel (AISI 304) sample by an f-theta lens with a focal length of 160 mm, to a waist diameter of 48 µm. Simultaneously, an X-ray beam with a diameter of approximately 2 mm was transmitted through the stainless-steel sample in a direction normal to the incident laser beam (y-direction in the coordinate system shown in Fig. 2). Behind the sample, a scintillator converts the X-ray beam into visible light, which is recorded by means of a high-speed camera at a framerate of 1000 fps and with a spatial resolution of 856 pixels/mm. The lateral dimensions of the X-ray beam limited the maximum depth of a borehole that can be accurately recorded to around 2 mm. The attenuation of the X-ray beam depends on the thickness of the irradiated metal. In areas where the air- and vapor-filled borehole in the sample reduces this thickness, the X-ray beam is less attenuated, thus resulting in a higher grayscale value recorded by the high-speed camera.

Drilling was performed with an ultrafast Yb:YAG laser (Carbide-CB3-80 from Light Conversion) with a pulse duration of 1 ps, a repetition rate of 50 kHz, and a wavelength of 1030 nm. Pulse energies E_P of 100 µJ, 150 µJ, and 400 µJ were used, resulting in fluences of 11.1 J/cm^2, 16.6 J/cm^2, and 44.2 J/cm^2, respectively. To investigate the influence of the polarization, experiments were conducted with.

a) linear polarization perpendicular to the plane of the X-ray images, (parallel to y-direction in Fig. 2),
b) linear polarization parallel to the plane of the X-ray images, (parallel to x-direction in Fig. 2), and
c) circular polarization.

The polarization at the sample was adjusted by means of λ/4 and λ/2 waveplates. The total drilling time was $t = 10$ s, which resulted in a total of $N_{max} = 500{,}000$ applied laser pulses. All experiments were performed in ambient air at atmospheric pressure.

3. Results and discussion

3.1. Side channels grow perpendicular to the direction of polarization

Fig. 3 shows X-ray images of three holes recorded after 10 s of drilling with different polarization states and a pulse energy of $E_P = 150$ µJ. The images reveal side channels growing parallel to the image plane when drilling with the polarization perpendicular to the image plane (Fig. 3a). Turning the polarization by 90° results in side channels which

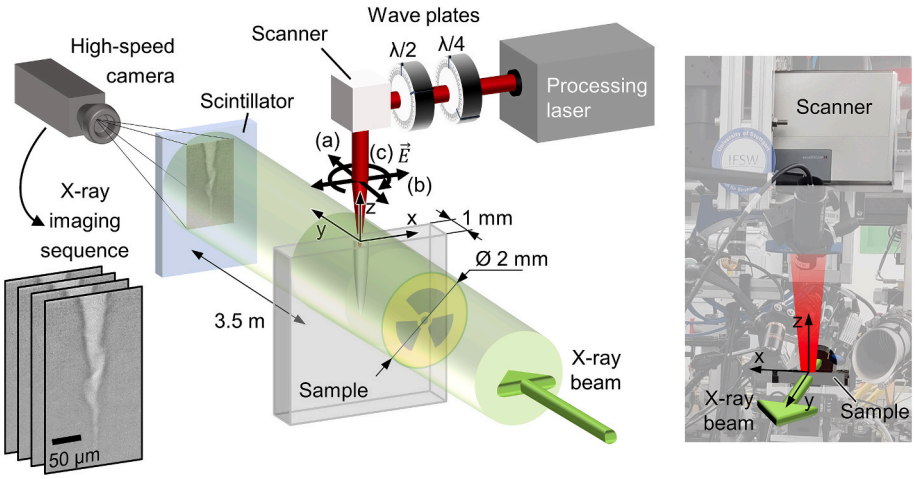

Fig. 2. Experimental X-ray imaging setup at DESY. Depiction based on [37] under CC-BY license.

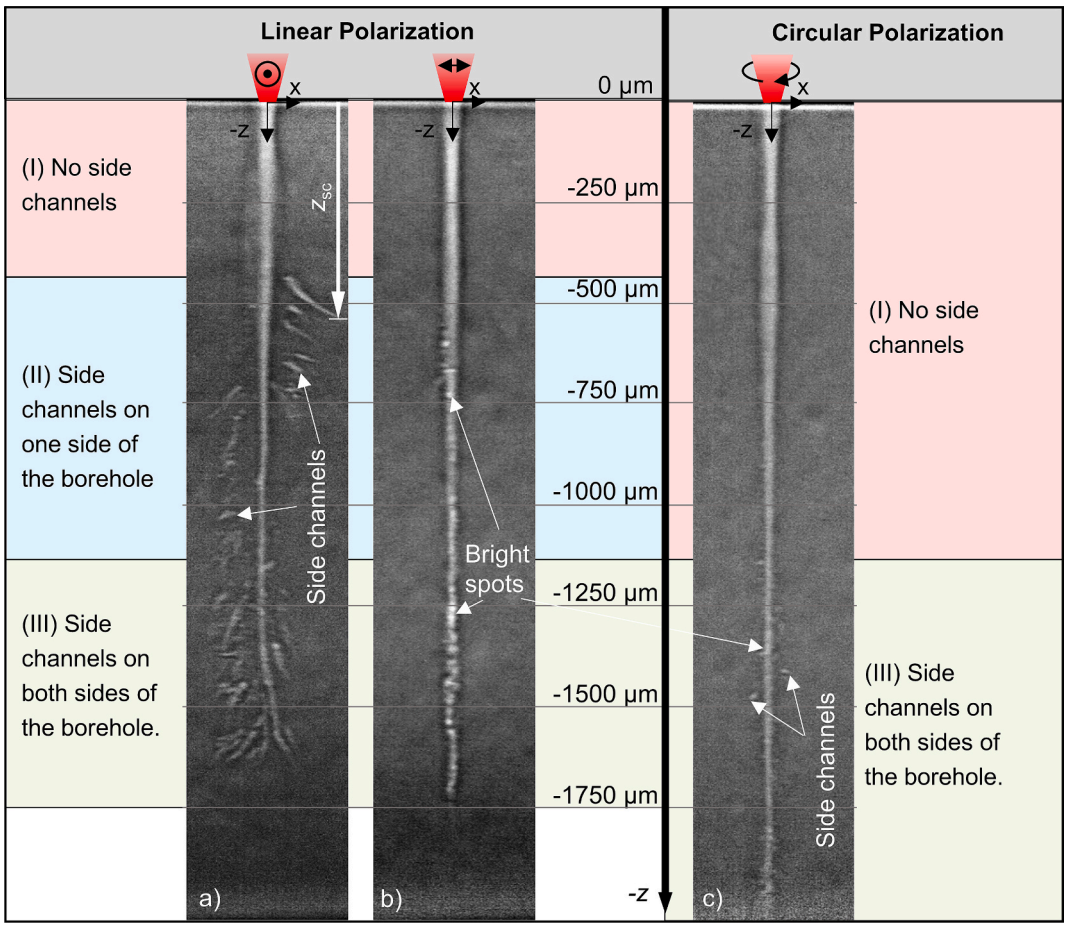

Fig. 3. Three different boreholes in stainless steel after $t = 10$ s i.e. $N = 500{,}000$ pulses drilled with a pulse energy of $E_P = 150$ µJ and different polarization states. a) Linear polarization perpendicular to the image plane. b) Linear polarization parallel to the image plane. c) Circular polarization. z_{sc} marks the position of the first side channel tip.

are oriented perpendicular to the image plane and can therefore only be detected by the local increase of the grayscale values along the borehole axis in Fig. 3b. The hole shown in Fig. 3c, which was drilled with circular polarization, shows fewer and shorter side channels. Note that these occur at greater depths compared to the side channels in the holes drilled with linear polarization. Apart from the visible side channels in the image plane, the bright spots on the axis of the borehole also reveal side channels that are oriented perpendicular to the plane of observation. The fact that the visible side channels appear to be shorter may be the result of their arbitrary orientation with respect to the image plane.

Closer examination shows that the side channels are distributed differently with increasing depth, which is indicated by the background colors in Fig. 3. During the initial drilling phase (Phase I, red), no side channels are visible. Phase II (blue) is characterized by asymmetrically formed side channels produced on only one side of the borehole at a time, and these were only observed when drilling with linear polarization. In the final phase III (green), the side channels were formed on both sides for both linear and circular polarization.

Comparison of the images in Fig. 3 indicates a direct correlation between linear polarization and the orientation of side channels in stainless steel, which is consistent with findings in PMMA by Xia et al. [8] and in diamond by Kononenko et al. [30]. From this it is clear that side channels primarily form in the plane perpendicular to the orientation of the linear polarization even in holes with aspect ratio > 30. The cavities show comparable geometries to those presented in other works for smaller aspect ratios [9,38]. However, the results presented here are the first evidence of side channels in boreholes with such high aspect ratios.

As shown in Fig. 3, the side channels develop at a significant distance to the borehole inlet independent of the polarization state. The position z_{sc} of the first side channel formed during drilling with linear polarization is presented in Fig. 4 as a function of pulse energy E_P. The red data points denote the average positions of the initial side channels in each hole, while black diamonds mark the individual data points. Arrows indicate the growth orientation of side channel, which appears to be randomly on the left or right. Notably, higher pulse energies correlate with greater depths of the first side channel.

Fig. 5 illustrates the details related to the (multiple) reflections of linearly polarized radiation propagating down a conically shaped hole. The middle picture showing the top view of the hole shows that the linearly polarized incident radiation is p-polarized with respect to the walls at positions A (blue) and s-polarized at positions B (orange). Fig. 6 shows the corresponding Fresnel reflectivity for both polarization states as a function of the angle of incidence. According to Fresnel's equations [39], the reflectivity R is lower at the walls where the incident radiation is p-polarized (blue) and higher at the walls with s-polarized radiation (orange), resulting in more intense reflected radiation along the B–B plane. This suggests that more energy is transported deeper into the borehole along the B–B plane, as illustrated by the thicker red arrows. After multiple reflections, this leads to a locally increased intensity in that plane, as demonstrated in [24,25]. This anisotropic energy distribution provides a plausible explanation for the preferential formation of side channels in the plane perpendicular to the polarization, as observed in Fig. 3.

In the following section, drilling experiments conducted with linearly polarized laser beams are analyzed to investigate the underlying

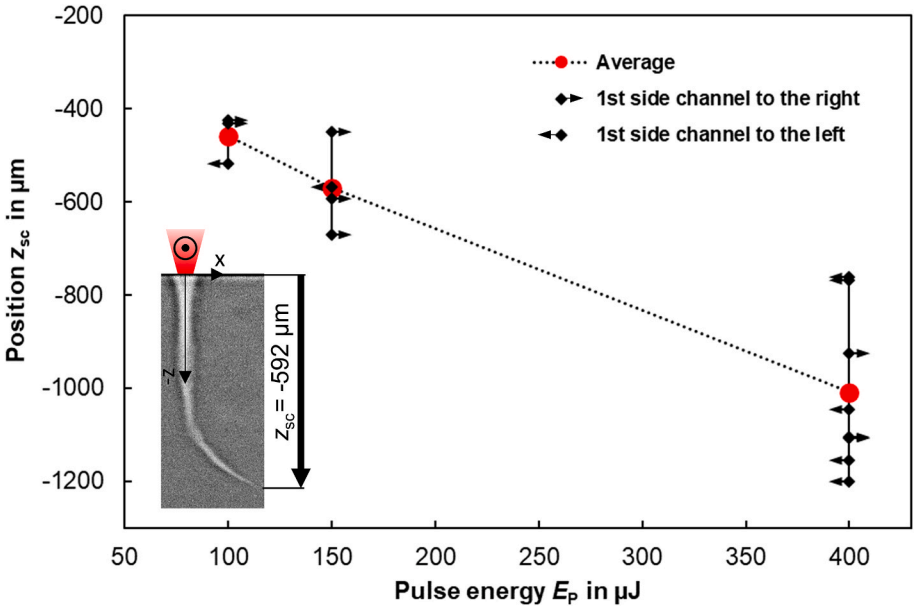

Fig. 4. Position z_{sc} of the first side channel formed during drilling with linear polarization as a function of the pulse energy E_P. The polarization is perpendicular to the observation plane depicted in the inset. The Red dots are the average of all measurements (black diamonds) for each pulse energy. The arrows indicate the direction (left or right) to which the corresponding side channel was formed. The dotted line is a guide to the eye only. The inset shows a side channel that was formed to the right during drilling with a pulse energy of E_P = 150 µJ.

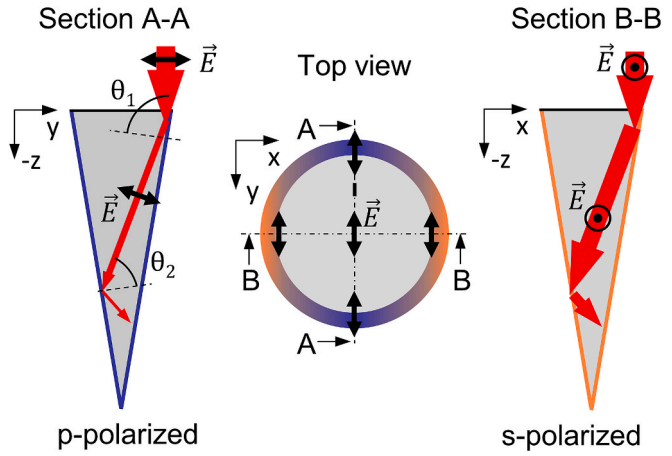

Fig. 5. Polarization states and ray propagation inside the borehole. Cross-section A-A: p-polarized (blue) and cross-section B-B: s-polarized (orange).

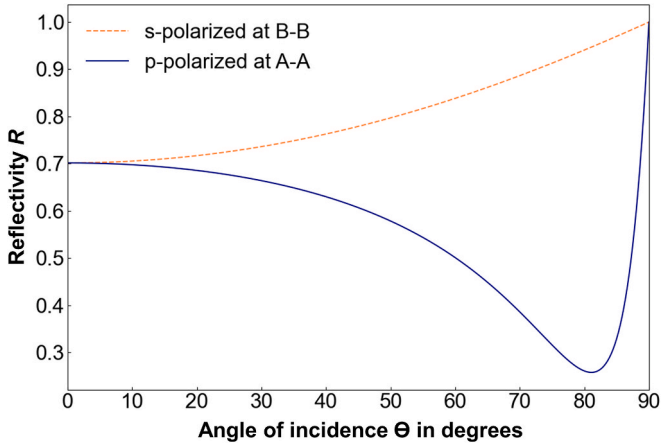

Fig. 6. Reflectivity R over angle of incidence Θ for stainless steel calculated with n = 3.76 and k = 5.27 [40].

mechanisms that lead to side channel formation. Two distinct phenomena will be presented and discussed in detail, based on time-resolved X-ray observations.

3.2. *Two distinct phenomena governing side channel formation*

Based on time-resolved X-ray image sequences, two different recurring phenomena governing the evolution of side channels were observed.

3.2.1. *Deflection of the borehole tip (Phenomenon D)*

Fig. 7 illustrates the formation of the first side channel in the hole shown previously in Fig. 3a. For $N \leq$ 6,500, the drilling proceeds vertically. In the upper region of the borehole ($z > -300$ µm), constantly changing structures are clearly visible on the borehole walls, as indicated by the white arrows. These structures lead to a dynamic redistribution of the laser radiation, as the angle of incidence and hence the local reflectivity R vary continuously along the borehole wall. As illustrated in Fig. 5, the reflectivity is higher in the plane perpendicular to the polarization direction, reinforcing an asymmetric energy distribution. This fluctuating pattern extends to the tip region, resulting in a gradual deflection of the tip as indicated by the black arrows in Fig. 7. These show subtle shifts in drilling direction up to N = 7,500 pulses, after which a pronounced deflection to the right occurs, marking the onset of side channel formation. According to Fig. 4, the lateral direction of side channels – left or right – is random; in the present case, the right side prevails. As the deflection increases, the borehole wall gradually moves out of the original beam path on that side (blue, inset at N = 8,500 Fig. 7). This causes the laser radiation to be predominantly reflected on the opposite wall (orange), focusing the energy input into the deflected tip and amplifying the deflection further. The growth of the side channel terminates at about N = 14,500, likely due to the emergence of melt-induced obstructions above the tip, which redirect the laser energy and alter the growth dynamics. The obstruction-driven behavior, referred to as Phenomenon O, is analyzed in the next section.

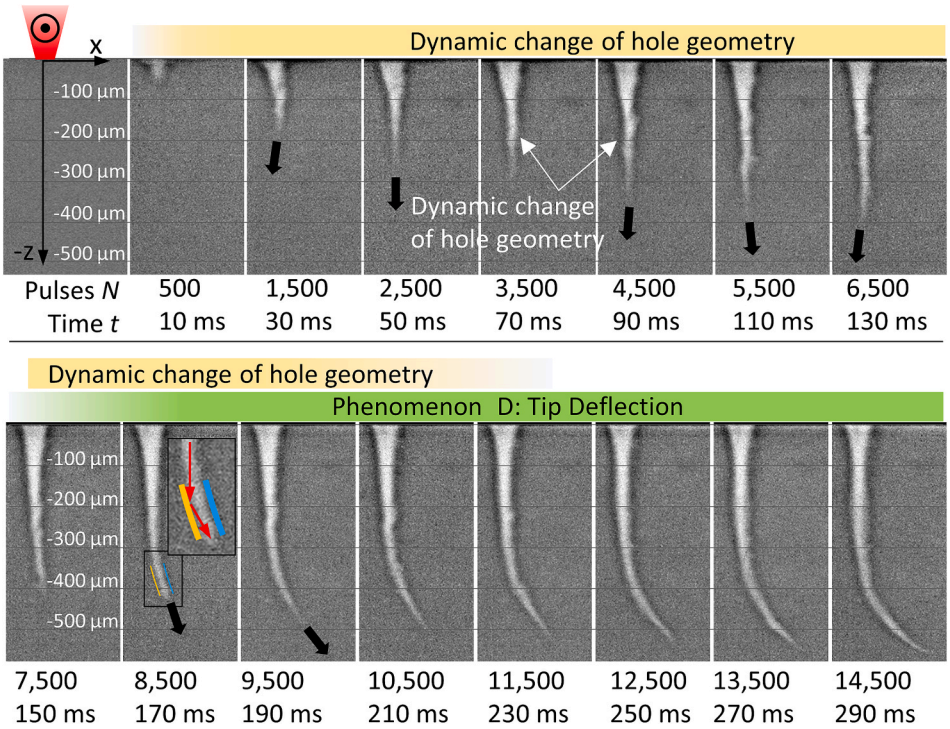

Fig. 7. Time-resolved X-ray image sequence showing the formation of the first side channel in the same borehole as in Fig. 3a. E_P = 150 µJ. The polarization is perpendicular to the image plane. The black arrows indicate the progression and orientation of the borehole tip. The blue line highlights the wall region that gradually moves out of the beam path as the tip deflects. The orange line indicates the side on which the laser radiation is predominantly reflected into the tip.

3.2.2. Melt-Induced obstructions above the borehole tip (Phenomenon O)

This phenomenon is visible in Fig. 8, which continues the sequence shown in Fig. 7. For $N \geq 14{,}500$ the side channel no longer grows significantly, neither to the side nor in depth. Instead, for $N \geq 15{,}500$ the borehole geometry between $z = -400$ µm and $z = -500$ µm begins to deviate from the path of the side channel, and irregularities appear that are likely caused by melt transported from the borehole tip. These melt-induced obstructions block the laser radiation from reaching the tip. As a result, the drilling process resumes closer to the original z-axis, as seen by the formation of a new channel at $N = 16{,}000$.

This new channel gradually seals off the previously formed side channel, disconnecting it from the main borehole, which becomes evident by $N = 18{,}500$. Drilling continues at the deepest part of the new (slightly right-deflected) tip of the main borehole, as indicated by the black arrow. From now on the process just described is repeated. The deflection of the tip increases again, which ultimately leads to a new side channel disconnected from the main borehole. As seen in the left borehole of Fig. 3 within the range -500 µm $> z > -750$ µm, successive side channels tend to align with the initial deflection direction. As such, the termination of one (side) channel is related to the effect starting a new channel. Both the initial formation and the eventual sealing of side channels appear to be linked to the presence of melt and the associated local geometric deviations.

The sequence in Fig. 7 and Fig. 8 illustrates a drilling process that transitions from an initial straight growth ($N < 7{,}500$) to a tip deflection (Phenomenon D), followed by an obstruction-driven interruption (Phenomenon O).

The following discussion describes a different progression, where side channel formation is first initiated by obstruction effects (Phenomenon O) and later governed by tip deflection (Phenomenon D).

3.3. Independent Occurrence and Variable sequence of both phenomena

Fig. 9 shows an image series illustrating the formation of a side

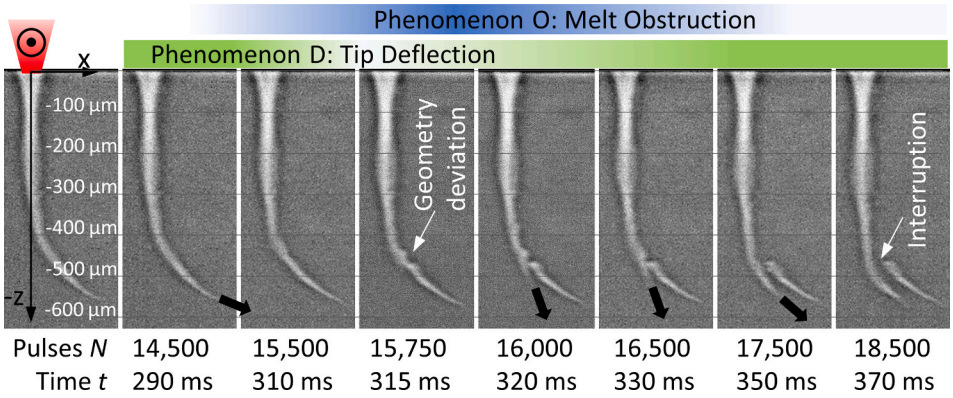

Fig. 8. Continuation of the time-resolved X-ray image sequence shown in Fig. 7, illustrating melt-induced cessation of side channel's growth. E_P = 150 µJ. The polarization is perpendicular to the image plane. The black arrows indicate the direction of the drilling progress.

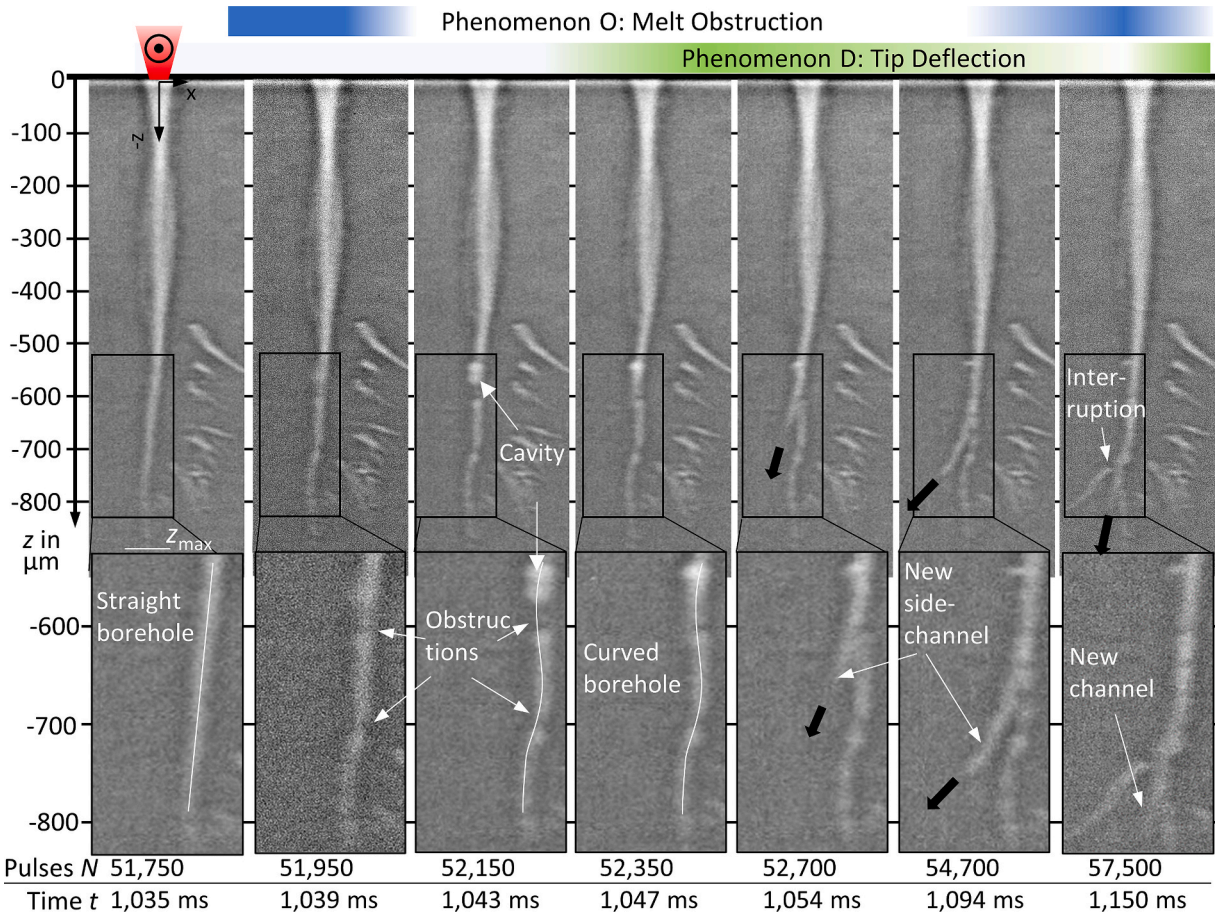

Fig. 9. Time-resolved X-ray image sequence showing the formation of a side channel induced by melt-related obstructions in the same borehole previously shown in Fig. 3a. $E_P = 150$ µJ. The polarization is perpendicular to the image plane. The black arrows indicate the growth direction of the (side) channel. The white arrows highlight obstructions, and the white line traces the evolving borehole geometry, which becomes increasingly curved due to melt redeposition.

channel caused by melt-induced obstructions in the same borehole already shown above, drilled with linear polarization perpendicular to the observation plane, and a pulse energy $E_P = 150$ µJ. In the first picture taken after $N = 51{,}750$ pulses, the borehole appears straight and the tip points downwards without a significant lateral deflection.

By $N = 51{,}950$ pulses, drilling at the tip ceases and two obstructions appear above the tip at $z = -600$ µm and $z = -700$ µm visible as dark areas, as pointed out by the white arrows. The borehole geometry becomes increasingly curved between -550 µm $> z > -800$ µm, as indicated by the white line in the fourth picture. These curvatures, together with the onset of obstructions, point to a local accumulation of melt along the borehole walls. The morphology of the borehole changes rapidly due to dynamic melt accumulation, which can lead to partial or complete obstruction or sealing of the channel. Such obstructions impede the propagation of the laser beam toward the borehole tip and causes a redistribution of energy within the borehole.

Consequently, after N = 52,150 pulses, the cavity formed just above z = −550 µm (as seen by the bright spot in the picture) evolves to form a new side channel, as clearly seen after $N = 52{,}700$ pulses and indicated by the black arrow. The formation to the left is presumably favored by the slightly left-angled borehole between -450 µm $> z > -550$ µm.

At this point, the further development of the side channel is governed by the same deflection-driven behavior described earlier as Phenomenon D. Around $N = 57{,}500$ pulses the growth of the side channel terminates, and drilling resumes closer to the laser axis forming a new channel which leads to the sealing of the just formed side channel.

The three presented image series in Fig. 7–Fig. 9 demonstrate that both phenomena can occur independently of each other and in different sequences.

The X-ray image sequences of this study clarify the origin of the side channels which result in reduced quality in case of drilling deep holes above the aspect ratio limit determined by Förster et al. [41]. A better understanding of the causes of unwanted geometry deviations is important for improving the percussion drilling process for deep holes used in various industrial applications [42].

4. Conclusion

High-speed X-ray imaging enabled real-time observation of the formation of side channels during percussion drilling with ultrashort laser pulses with different polarization conditions. This provides key insights into transient effects influencing the eventual borehole geometry.

The following conclusions can be drawn from this study:

- Side channels predominantly form in the plane perpendicular to the polarization direction of linearly polarized light. Their initial lateral growth direction (left or right) is random but subsequent channels tend to be grouped to the same side.
- Higher pulse energies shift the location of the initial side channel to greater depths.
- Two distinct phenomena were identified that govern the formation of side channels:
- (1) Tip deflection (Phenomenon D), where the borehole tip deviates laterally due to the polarization-dependent asymmetric reflection of the incident radiation;

- (2) Melt-induced obstructions (Phenomenon O), where accumulated melt above the borehole tip alters the local geometry and angle of incidence, interrupting axial drilling and redistributing energy laterally, thereby initiating the formation of side channels.
- These mechanisms occur independently and in varying order
- Side channels can persist as voids disconnected from the main borehole, potentially affecting the function of the drilled component.

Further research is required to explore the underlying mechanisms in more detail e.g. using raytracing methods and numerical simulation of the fluid dynamics, which may potentially provide indications for new approaches to influence the process of percussion drilling.

For future research in this field, the detection capability of the equipment could be improved by integrating next-generation high-speed imaging systems offering improved light sensitivity and better pixel resolution. Furthermore, the reflectivity and absorption properties of different materials, such as metals or polymers, can significantly influence side channel formation dynamics. These materials have different optical and thermal characteristics, which in turn affect energy deposition and melt behavior. Future research could expand the present study by including additional materials, thereby allowing researchers to generalize the results.

CRediT authorship contribution statement

Lukas Schneller: Writing – review & editing, Writing – original draft, Visualization, Methodology, Investigation, Data curation, Conceptualization. **Manuel Henn:** Investigation. **Marc Hummel:** Project administration, Investigation. **Christoph Spurk:** Investigation. **Felix Beckmann:** Investigation. **Julian Moosmann:** Investigation. **Alexander Olowinsky:** Funding acquisition. **Daniel Holder:** Writing – review & editing. **Christian Hagenlocher:** Writing – review & editing, Supervision, Funding acquisition, Conceptualization. **Thomas Graf:** Writing – review & editing, Supervision, Funding acquisition, Conceptualization.

Declaration of competing interest

The authors declare that they have no known competing financial interests or personal relationships that could have appeared to influence the work reported in this paper.

Acknowledgements

This work was supported by the Landesministerium für Wissenschaft, Forschung und Kunst Baden-Württemberg (Ministry of Science, Research and the Arts of the State of Baden-Württemberg) within the Nachhaltigkeitsförderung (sustainability support) of the projects of the Exzellenzinitiative II. The presented investigations were carried out within the cooperation “Laser Meets Synchrotron” (www.laser-meets-synchrotron.de). The experimental setup and its operation were funded by the Deutsche Forschungsgemeinschaft e.V. (DFG, German Research Foundation) within the framework of the Collaborative Research Centre SFB1120-236616214 “Bauteilpräzision durch Beherrschung von Schmelze und Erstarrung in Produktionsprozessen”. The experiments were carried out in cooperation with Helmholtz-Zentrum Hereon in Hamburg at Beamline P07 of DESY PETRA III as part of proposal BAG-20211050 and we would like to thank F. Beckmann, J. Moosmann and all people involved for their support. Thanks to Light Conversion (Vilnius, Lithuania) for providing the ultrafast laser (Carbide CB3 80) and to Anne Feuer for the SEM image.

Data availability

The processed data required to reproduce these findings are available online at https://doi.org/10.18419/DARUS-5086 [43]. The data contains a synchrotron X-ray image sequence of a laser percussion drilling process.

References

[1] T. Beck, Laser drilling in gas turbine blades, LTJ 8 (2011) 40–43, https://doi.org/10.1002/latj.201190024.
[2] C.A. McNally, J. Folkes, I.R. Pashby, Laser drilling of cooling holes in aeroengines: state of the art and future challenges, Mater. Sci. Technol. 20 (2004) 805–813, https://doi.org/10.1179/026708304225017391.
[3] M. Henn, G. Reichardt, R. Weber, et al., Dry metal forming using volatile lubricants injected into the forming tool through flow-optimized, Laser-Drilled Microholes. JOM 72 (2020) 2517–2524, https://doi.org/10.1007/s11837-020-04169-6.
[4] S. Döring, S. Richter, S. Nolte, et al., In situ imaging of hole shape evolution in ultrashort pulse laser drilling, Opt. Express 18 (2010) 20395–20400, https://doi.org/10.1364/OE.18.020395.
[5] H. Hidai, Y. Kuroki, S. Matsusaka, et al., Curved drilling via inner hole laser reflection, Precis. Eng. 46 (2016) 96–103, https://doi.org/10.1016/j.precisioneng.2016.04.004.
[6] Y. Zhang, S. Li, G. Chen, et al., Experimental observation and simulation of keyhole dynamics during laser drilling, Opt. Laser Technol. 48 (2013) 405–414, https://doi.org/10.1016/j.optlastec.2012.10.039.
[7] T.V. Kononenko, S.M. Klimentov, S.V. Garnov, et al., Hole formation process in laser deep drilling with short and ultrashort pulses, in: I. Miyamoto, Y.F. Lu, K. Sugioka (Eds.), Second International Symposium on Laser Precision Microfabrication. SPIE, p 108, 2001.
[8] B. Xia, L. Jiang, X. Li, et al., Mechanism and elimination of bending effect in femtosecond laser deep-hole drilling, Opt. Express 23 (2015) 27853–27864, https://doi.org/10.1364/OE.23.027853.
[9] W. Zhao, X. Shen, H. Liu, et al., Effect of high repetition rate on dimension and morphology of micro-hole drilled in metals by picosecond ultra-short pulse laser, Opt. Lasers Eng. 124 (2020) 105811, https://doi.org/10.1016/j.optlaseng.2019.105811.
[10] Feuer A, Kunz C, Kraus M et al.: Influence of laser parameters on quality of microholes and process efficiency. In: Nakata Y, Xu X, Roth S et al. (eds) Laser Applications in Microelectronic and Optoelectronic Manufacturing (LAMOM) XIX, 89670H (2014).
[11] Arnold T, Götter P, Wanke D et al.: High-speed process observation of pulsed laser drilling in non-transparent materials (2017).
[12] M. Chen, Y. Wang, G. Yu, et al., In situ optical observations of keyhole dynamics during laser drilling, Appl. Phys. Lett. 103 (2013), https://doi.org/10.1063/1.4829147.
[13] Y. Zhang, X. He, G. Yu, et al., Dynamic evolution of keyhole during multi-pulse drilling with a millisecond laser on 304 stainless steel, Opt. Laser Technol. 152 (2022) 108151, https://doi.org/10.1016/j.optlastec.2022.108151.
[14] Michalowski A, Qin Y, Weber R et al.: Theoretical and experimental studies of ultra-short pulsed laser drilling of steel. In: Mackenzie JI, Jelínková H, Taira T et al. (eds) Laser Sources and Applications II, 91350R (2014).
[15] A. Michalowski, Melt dynamics and hole formation during drilling with ultrashort pulses, JLMN 3 (2008) 211–215, https://doi.org/10.2961/jlmn.2008.03.0015.
[16] T.V. Kononenko, C. Freitag, D.N. Sovyk, et al., Influence of pulse repetition rate on percussion drilling of Ti-based alloy by picosecond laser pulses, Opt. Lasers Eng. 103 (2018) 65–70, https://doi.org/10.1016/j.optlaseng.2017.12.003.
[17] W. Zhao, Z. Yu, Self-cleaning effect in high quality percussion ablating of cooling hole by picosecond ultra-short pulse laser, Opt. Lasers Eng. 105 (2018) 125–131, https://doi.org/10.1016/j.optlaseng.2018.01.011.
[18] Mikheev GM, Idiatulin VS: Influence of light polarization on laser destruction. In: Akos G, Lupkovics G, Podmaniczky A (eds) OPTIKA ’98: 5th Congress on Modern Optics. SPIE, p 36 (1998).
[19] Z. Yan, X. Mei, W. Wang, et al., Theoretical investigation of multipulse femtosecond laser processing on silicon carbide: ablation, shielding effect, and recast formation, Opt. Laser Technol. 181 (2025) 111976, https://doi.org/10.1016/j.optlastec.2024.111976.
[20] Z. Zhang, W. Wang, R. Jiang, et al., Investigation on geometric precision and surface quality of microholes machined by ultrafast laser, Opt. Laser Technol. 121 (2020) 105834, https://doi.org/10.1016/j.optlastec.2019.105834.
[21] Z. Zhang, Z. Xu, C. Wang, et al., Molecular dynamics-guided quality improvement in the femtosecond laser percussion drilling of microholes using a two-stage pulse energy process, Opt. Laser Technol. 139 (2021) 106968, https://doi.org/10.1016/j.optlastec.2021.106968.
[22] X. Sun, X. Dong, K. Wang, et al., Femtosecond laser processing of controlled tapered micro-holes based on dynamic control of relative attitude, Opt. Laser Technol. 170 (2024) 110201, https://doi.org/10.1016/j.optlastec.2023.110201.
[23] J. Jiang, M. Chen, Z. Bai, et al., Influence of polarization on the hole formation with picosecond laser, Opt. Rev. 20 (2013) 496–499, https://doi.org/10.1007/s10043-013-0084-4.
[24] A. Zhanwen, Z. Guisheng, W. Zhao, et al., The mechanism of irregular hole-shape formation during ultrafast laser micro-drilling of metals, Appl. Phys. A 129 (2023), https://doi.org/10.1007/s00339-022-06358-3.
[25] S. Nolte, C. Momma, G. Kamlage, et al., Polarization effects in ultrashort-pulse laser drilling, Appl. Phys. A 68 (1999) 563–567, https://doi.org/10.1007/s003390050941.
[26] R. Wang, X. Dong, K. Wang, et al., Polarization effect on hole evolution and periodic microstructures in femtosecond laser drilling of thermal barrier coated

superalloys, Appl. Surf. Sci. 537 (2021) 148001, https://doi.org/10.1016/j.apsusc.2020.148001.
[27] C. Foehl, F. Dausinger, High precision deep drilling with ultrashort pulses, in: I. Miyamoto, A. Ostendorf, K. Sugioka (Eds.), Fourth International Symposium on Laser Precision Microfabrication. SPIE, 2003 p 346.
[28] L. Schneller, M. Henn, C. Spurk, et al., High-speed X-ray imaging of bulge formation during laser percussion drilling with various polarizations in stainless steel, Procedia CIRP 124 (2024) 644–648, https://doi.org/10.1016/j.procir.2024.08.192.
[29] A. Zhanwen, G. Zou, H. Yu, et al., Polarization-dependent, beam reflection-regulated hole shaping dynamics visualized by in-situ imaging of ultrafast laser drilling process, Precis. Eng. 86 (2024) 153–159, https://doi.org/10.1016/j.precisioneng.2023.11.010.
[30] T.V. Kononenko, V.I. Konov, Dynamics of deep short pulse laser drilling: ablative stages and light propagation, Laser Phys. 11 (2001) 343–351.
[31] K. Venkatakrishnan, B. Tan, P. Stanley, et al., The effect of polarization on ultrashort pulsed laser ablation of thin metal films, J. Appl. Phys. 92 (2002) 1604–1607, https://doi.org/10.1063/1.1487453.
[32] J.-H. Cho, S.-J. Na, Theoretical analysis of keyhole dynamics in polarized laser drilling, J. Phys. D Appl. Phys. 40 (2007) 7638–7647, https://doi.org/10.1088/0022-3727/40/24/007.
[33] Henn M, Schneller L, Holder D et al.: Unveiling laser percussion drilling in metals with ultrashort pulses: insights from high-speed synchrotron x-ray imaging on microhole formation and side channel phenomena. In: Kling R, Pfleging W, Sugioka K (eds) Laser-based Micro- and Nanoprocessing XVIII. SPIE, p 19 (2024).
[34] M. Buser, M. Henn, L. Schneller, et al., Measuring the progress of laser drilling by means of OCT and validation using X-ray synchrotron imaging, Lasers Manuf. Mater. Process. (2025), https://doi.org/10.1007/s40516-025-00287-8.
[35] N. Schell, A. King, F. Beckmann, et al., The high energy materials science beamline (HEMS) at PETRA III, MSF 772 (2013) 57–61, https://doi.org/10.4028/www.scientific.net/MSF.772.57.
[36] J. Wagner, C. Hagenlocher, M. Hummel, et al., Synchrotron X-ray analysis of the influence of the magnesium content on the absorptance during full-penetration laser welding of aluminum, Metals 11 (2021) 797, https://doi.org/10.3390/met11050797.
[37] L. Schneller, M. Henn, M. Buser, Setup for High-speed synchrotron X-ray imaging of laser drilling at the DESY, V1 DaRUS (2024).
[38] S. Döring, J. Szilagyi, S. Richter, et al., Evolution of hole shape and size during short and ultrashort pulse laser deep drilling, Opt. Express 20 (2012) 27147–27154, https://doi.org/10.1364/OE.20.027147.
[39] A.-J. Fresnel: Mémoire sur la loi des modifications que la réflexion imprime à la lumière polarisée: Memoir on the law of the modifications that reflection impresses on polarized light (1834).
[40] M.N. Polyanskiy, Refractiveindex.info database of optical constants, Sci. Data 11 (2024) 94, https://doi.org/10.1038/s41597-023-02898-2.
[41] D.J. Förster, R. Weber, D. Holder, et al., Estimation of the depth limit for percussion drilling with picosecond laser pulses, Opt. Express 26 (2018) 11546–11552, https://doi.org/10.1364/OE.26.011546.
[42] U. Dürr, Laser Drilling in Industrial Use, Laser Tech. J. 5 (2008) 57–59, https://doi.org/10.1002/latj.200890029. doi: 10.18419/DARUS-5086.

Further reading

[43] L. Schneller, M. Henn, et al., Supplementary Data for Paper "Polarization-Dependent Formation of Side Channels During Percussion Drilling with Ultrafast Lasers Observed by Means of High-Speed X-Ray Imaging, DARUS (2025), https://doi.org/10.18419/DARUS-5086.